Sensors & Actuators: B. Chemical 473 (2027) 141245

Contents lists available at ScienceDirect

Sensors and Actuators: B. Chemical

journal homepage: www.elsevier.com/locate/snb

η-shaped dual-resonance acoustic resonator for dual-gas QEPAS using a single quartz tuning fork

Zhen Zhang [a,1], Chenzhao Sang [a,1], Haiyue Sun [a], Chu Zhang [a], Shunda Qiao [a], Hong Qi [b], Angelo Sampaolo [c], Vincenzo Spagnolo [c], Yufei Ma [a,*], Ying He [a,b,**]

[a] National Key Laboratory of Laser Spatial Information, Harbin Institute of Technology, Harbin 150000, China
[b] School of Energy Science and Engineering, Harbin Institute of Technology, Harbin 150000, China
[c] PolySense Lab—Dipartimento Interateneo di Fisica, Politecnico di Bari, Italy

ARTICLE INFO

Keywords:
Quartz-enhanced photoacoustic spectroscopy (QEPAS)
Dual-resonance acoustic resonator
Fundamental- and overtone-mode frequency multiplexing

ABSTRACT

We developed a novel dual-gas quartz-enhanced photoacoustic spectroscopy (QEPAS) sensor based on an η-shaped dual-resonance acoustic resonator and a low-frequency quartz tuning fork (QTF). The fundamental and overtone modes of the QTF, with resonance frequencies of 2964.4 and 18294.0 Hz, respectively, were employed as two independent frequency channels for simultaneous gas sensing. The η-shaped resonator was designed to provide acoustic resonance enhancement for both channels. Acetylene (C_2H_2) and methane (CH_4) were selected as the target gases. Compared with the bare-QTF configuration, the second harmonic (2 *f*) signal amplitudes of C_2H_2 and CH_4 were enhanced by 16.3 and 12.0 times, respectively. The two sensing channels show excellent linear concentration responses with $R^2 > 0.99$, and no inter-channel crosstalk is observed. Allan deviation-derived minimum detection limits were 148.7 ppb for C_2H_2 and 155.0 ppb for CH_4. Such results confirm that the proposed η-geometry dual-resonance acoustic resonator constitutes a straightforward and efficient solution for sensitivity enhancement of single-QTF frequency-multiplexed QEPAS sensors in multi-gas analysis.

1. Introduction

Highly sensitive detection of multiple gas species has significant application value across a wide range of fields, including atmospheric monitoring, industrial process control, combustion diagnostics, and environmental sensing [1–13]. Laser-based gas sensing techniques have been extensively investigated due to their high selectivity, high sensitivity, and rapid response [14–26]. As one of the laser-based spectroscopic techniques, photoacoustic spectroscopy (PAS) has attracted widespread attention owing to its merits including zero-background detection, laser wavelength-independent measurement, and compact volume [27–38]. Quartz-enhanced photoacoustic spectroscopy (QEPAS) represents a major advance over conventional microphone-based PAS. QEPAS employs a quartz tuning fork (QTF) as a sharply resonant acoustic transducer to detect the acoustic wave generated by the photoacoustic effect. The high quality factor (Q-factor), narrow response bandwidth, small size, and low cost of the QTF make it particularly suitable for compact trace-gas sensing [39–41]. In addition, compared with conventional microphone-based photoacoustic spectroscopy, the extremely narrow frequency response of the QTF delivers superior suppression of ambient acoustic noise [42–44]. These characteristics have promoted the development of QEPAS sensors from single-gas detection toward multicomponent gas sensing [45–47].

Several approaches have been proposed and developed to realize multi-gas QEPAS sensing. A straightforward method is to employ a single widely tunable laser whose emission wavelength covers the absorption lines of different target gases [48,49]. However, this approach is limited by the wavelength tuning range of the laser, especially when the selected absorption lines are spectrally far apart. Alternatively, several lasers can be combined with a single QEPAS detection module, while optical switching or time-division multiplexing is used to sequentially detect different gas species [50,51]. Such a configuration extends the spectral coverage but does not allow continuous simultaneous detection. Another approach is to integrate multiple independent QEPAS sensing channels, with each channel targeting an individual gas component [52,53]. Although real simultaneous multi-gas sensing can

* Corresponding author.
** Corresponding author at: National Key Laboratory of Laser Spatial Information, Harbin Institute of Technology, Harbin 150000, China.
E-mail addresses: mayufei@hit.edu.cn (Y. Ma), hearkenyi@163.com (Y. He).
[1] These authors contributed equally to this work.

https://doi.org/10.1016/j.snb.2026.141245

Available online 16 November 2026
0925-4005/© 2026 Elsevier B.V. All rights are reserved, including those for text and data mining, AI training, and similar technologies.

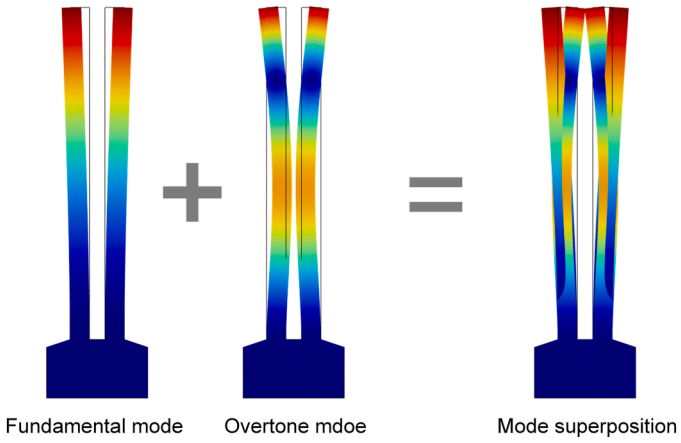


Fig. 1. The fundamental mode, the overtone mode and their fused dual-mode vibration of a QTF.

be achieved, the use of multiple QTFs and corresponding detection units inevitably increases the system size and complexity.

Frequency-division multiplexing provides an effective approach for simultaneous multi-gas QEPAS sensing by separating different gas signals into independent frequency channels [54–57]. The feasibility of this strategy has been demonstrated using different resonance modes of a single QTF. However, frequency multiplexing itself does not provide acoustic enhancement for each sensing channel. Acoustic resonators are widely employed in QEPAS to enhance the acoustic-wave intensity and improve the detection sensitivity [58]. However, a conventional acoustic resonator is generally designed for a single operating frequency. When two widely separated resonance frequencies are employed for frequency-multiplexed sensing, simultaneously achieving efficient resonance matching within a compact and integrated acoustic structure remains challenging. An acoustic resonator capable of supporting independently tailored resonances for both QTF modes is highly desirable for further improving the performance and compactness of frequency-multiplexed QEPAS sensors.

In this work, we develop a novel η-shaped dual-resonance acoustic resonator for a dual-gas QEPAS sensor using a single low-frequency QTF. The measured fundamental and overtone resonance frequencies of the QTF were 2964.4 and 18294.0 Hz, respectively. The η-shaped acoustic resonator consists of a buffer chamber and two acoustic resonator tubes with different lengths, where the long and short tubes are employed to provide acoustic resonance enhancement for the fundamental and overtone modes, respectively. Two distributed feedback diode lasers emitting at 1530.37 and 1650.96 nm were employed for acetylene (C_2H_2) and methane (CH_4) detection, respectively. Compared with a bare-QTF configuration, the C_2H_2 and CH_4 second harmonic (2 f) signal amplitudes were enhanced by 16.3 and 12.0 times, respectively. The two sensing channels exhibited good linear concentration responses without observable inter-channel crosstalk. Furthermore, Allan deviation analysis yielded minimum detection limits of 148.7 ppb for C_2H_2 at an integration time of 800 s and 155.0 ppb for CH_4 at 200 s. These results demonstrate that dual acoustic resonance enhancement can be effectively introduced into fundamental/overtone frequency-multiplexed QEPAS, providing a simple approach for improving the detection performance of compact single-QTF based multi-gas sensors.

2. Operating principle and dual-resonance acoustic resonator

2.1. Dual-mode operation of the QTF

A low-frequency QTF was employed as the acoustic transducer in the proposed dual-gas QEPAS sensor. In addition to the fundamental mode, a QTF possesses a series of higher-order flexural modes. Therefore, the fundamental and overtone modes of a single QTF can provide two frequency-separated acoustic detection channels. The feasibility of such a frequency-division multiplexing strategy has been demonstrated in QEPAS sensing, where gas-induced photoacoustic signals at different frequencies can be independently extracted using different QTF resonance modes. In the present work, the fundamental (f_0) and first

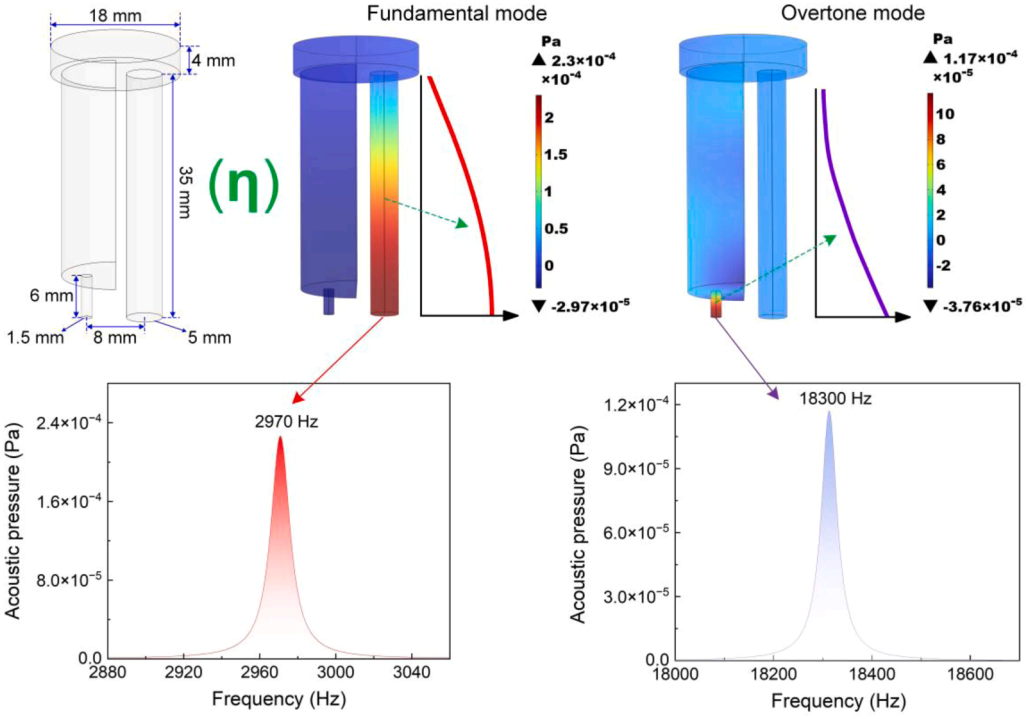


Fig. 2. Geometry and simulated acoustic characteristics of the η-shaped dual-resonance acoustic resonator, including the acoustic pressure distributions, frequency responses, and radial acoustic pressure distributions within the effective resonant cavities at 2970 Hz and 18300 Hz.

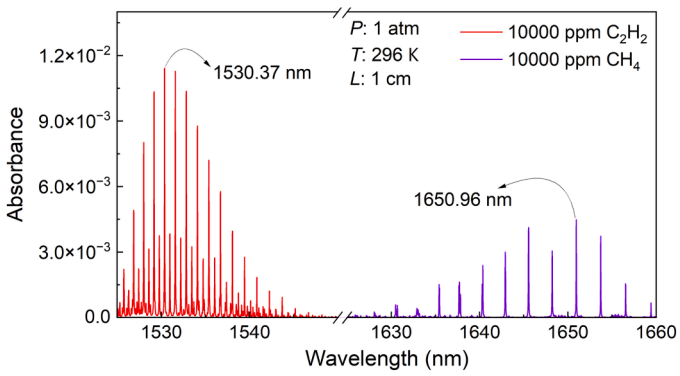


Fig. 3. Simulated absorption spectra of C_2H_2 and CH_4 in the near-infrared region.

overtone mode (f_1) of the low-frequency QTF were employed as two frequency channels. They can simultaneously exist and achieve modal linear superposition, as shown in Fig. 1. Their resonance frequencies were experimentally characterized before determining the corresponding modulation frequencies, as discussed in Section 4.1. The large frequency separation between the two mechanical modes provides natural frequency-domain isolation for simultaneous dual-gas sensing. However, the large difference between f_0 and f_1 also makes it difficult to enhance both photoacoustic signals using a conventional single-resonance acoustic resonator. To address this issue, a dual-resonance acoustic structure was developed, as described below.

2.2. Design of the dual-resonance η-shaped acoustic resonator

In a conventional QEPAS spectrophone, an acoustic resonator is generally designed to enhance the acoustic wave at a specific operating frequency. For the dual-mode QTF employed here, the fundamental and overtone frequencies of the QTF are widely separated, making it difficult for a conventional single-resonance acoustic resonator to efficiently enhance both channels. Therefore, an η-shaped acoustic resonator possessing two acoustic resonance modes was designed. As shown in Fig. 2, the resonator consists of a common buffer chamber and two resonator tubes with different dimensions. The resonator was fabricated from aluminum alloy using conventional mechanical machining techniques. The long and short branches are designed for the fundamental- and overtone-frequency channels, respectively.

Finite-element analysis was performed to investigate the acoustic characteristics of the η-shaped resonator. The computational mesh was refined to adequately resolve both acoustic resonance modes, particularly the higher-frequency mode. In the frequency-domain simulations, the photoacoustic excitation was represented by a distributed harmonic source along the laser propagation path to simulate the periodic excitation induced by gas absorption. As demonstrated in Fig. 2, two distinct longitudinal acoustic resonance modes were obtained at 2970 and 18300 Hz, with corresponding 3 dB bandwidths of 11.5 and 39.6 Hz, respectively. The lengths of the long and short resonator branches correspond to approximately 0.31 and 0.32 times their respective acoustic wavelengths, respectively. For the low-frequency mode, the acoustic pressure was mainly concentrated in the long resonator branch, whereas the high-frequency mode was primarily confined to the short branch. Furthermore, the radial acoustic pressure distributions within the corresponding effective resonant cavities were calculated as shown in Fig. 2, providing a more comprehensive visualization of the acoustic field characteristics of the two resonance modes.

Although the acoustic fields are predominantly localized in different branches, the two resonances represent distinct acoustic modes of the entire η-shaped cavity rather than independent resonances of two isolated tubes. The common buffer chamber provides acoustic coupling between the two branches and influences their effective acoustic boundary conditions, thereby contributing to the formation of both resonance modes. The simulated pressure distributions indicate relatively weak acoustic fields in the shared chamber, suggesting limited spatial overlap between the two modes. Nevertheless, their distinct spatial distributions and large frequency separation enable frequency-selective acoustic enhancement for the fundamental and overtone modes of the QTF.

3. Experiment setup

3.1. Absorption line selection

C_2H_2 and CH_4 were selected as the target gases to evaluate the simultaneous dual-gas sensing performance of the proposed QEPAS sensor. The absorption spectra of C_2H_2 and CH_4 in the near-infrared region were calculated based on the HITRAN database [59], as shown in Fig. 3. Two absorption lines located at 1530.37 nm for C_2H_2 and 1650.96 nm for CH_4 were selected for gas detection. The two target absorption lines are separated by approximately 121 nm and exhibit negligible spectral overlap, which effectively suppresses spectral interference between the two sensing channels. Furthermore, previous studies have demonstrated that the selected C_2H_2 and CH_4 absorption

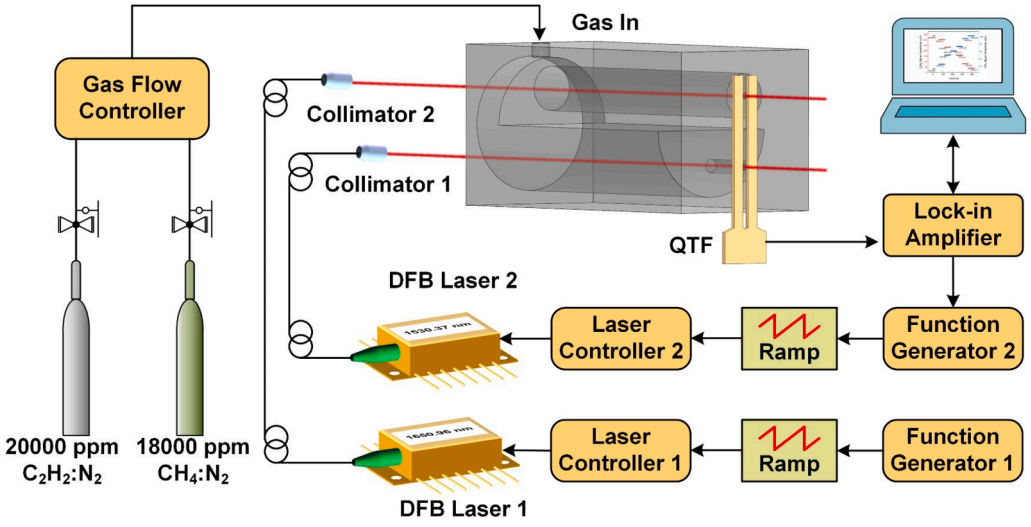


Fig. 4. Schematic diagram of the dual-gas QEPAS sensor system based on the η-shaped dual-resonance acoustic resonator.

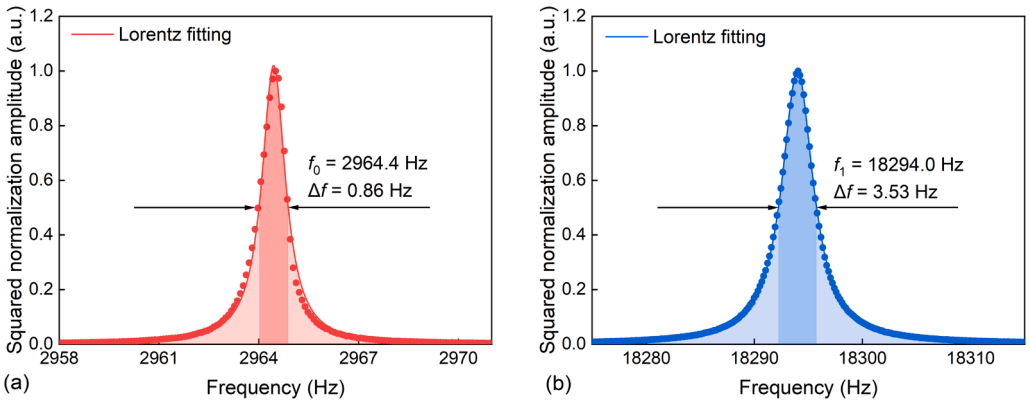


Fig. 5. Frequency responses of the QTF at (a) the fundamental mode for the C_2H_2 channel and (b) the overtone mode for the CH_4 channel.

lines exhibit minimal spectral interference from common atmospheric species, including H_2O and CO_2 [17,60,61]. Therefore, these absorption lines are suitable for selective dual-gas detection with limited interference from other gas species.

Two continuous-wave distributed feedback (DFB) diode lasers with emission wavelengths around 1530.37 and 1650.96 nm were employed, respectively. The two lasers were independently wavelength-modulated and assigned to the fundamental and overtone mode detection channels of the QTF. In this way, spectral selectivity is provided by the molecular absorption lines, while the two photoacoustic signals are further separated in the frequency domain by the two QTF resonance modes.

3.2. Dual-gas QEPAS sensor system

The experimental setup of the dual-gas QEPAS sensor based on the η-shaped acoustic resonator is shown in Fig. 4. Two continuous-wave DFB diode lasers, referred to as laser 1 and laser 2, were employed as the excitation sources for C_2H_2 and CH_4 detection, respectively. The output beams were collimated and introduced into the η-shaped acoustic resonator through an optical CaF_2 window, which was mounted on the resonator to provide optical access. The two laser beams were directed through the corresponding resonator branches, and their positions were kept unchanged during the measurements. Since the acoustic excitation efficiency depends on the spatial overlap between the laser-induced photoacoustic excitation and the corresponding acoustic resonance mode, appropriate beam alignment is important for efficient acoustic coupling. The optical powers of the two DFB lasers incident on the acoustic resonator were 10.06 mW and 13.51 mW for C_2H_2 and CH_4 detection, respectively.

The η-shaped resonator served simultaneously as the gas cell and the acoustic enhancement unit, while a single low-frequency QTF with a prong length of 17 mm, width of 1 mm and gap of 0.8 mm was employed to detect the enhanced photoacoustic signals. Two acoustic openings were arranged near the ends of the corresponding resonator branches. Considering the different displacement distributions of the fundamental and overtone modes, the acoustic outlets were positioned close to the corresponding vibration regions of the QTF prongs to facilitate efficient acoustic coupling. In this arrangement, the acoustic waves generated in the long and short branches could effectively excite the fundamental and overtone modes of the QTF, respectively.

The experiments were performed at ambient atmospheric pressure, without active pressure stabilization. During the concentration measurements, the gas mixtures were prepared using mass-flow controllers, with the total flow rate maintained at 60 mL/min. Wavelength modulation spectroscopy combined with 2*f* detection was employed to improve the detection signal-to-noise ratio. Low-frequency ramp signals (f_s=5 mHz) were applied to the two laser drivers to periodically scan the laser wavelengths across the corresponding gas absorption lines. Meanwhile, sinusoidal modulation signals were superimposed on the laser injection currents. According to the dual-mode operation described in Section 2.1, the modulation frequencies of laser 1 and laser 2 were set to half of the QTF fundamental and overtone frequencies, respectively.

The QTF output was subsequently demodulated at the fundamental and overtone frequencies to independently retrieve the two gas signals. The 2*f* signal amplitudes of both channels were extracted from the magnitude output of the lock-in amplifier, eliminating the need for independent adjustment of the lock-in reference phases. A time constant of 200 ms and a filter slope of 18 dB/oct were employed for both detection channels.

4. Results and discussion

4.1. Frequency characterization and modulation optimization

The resonance frequencies of the QTF are critical parameters for determining the modulation frequencies of the two sensing channels. Therefore, the frequency responses of the fundamental and overtone modes were first characterized using light-induced thermoelastic excitation. A sinusoidally modulated laser beam was directly irradiated onto the QTF surface to induce thermoelastic vibration. The modulation frequency was swept across the fundamental and overtone resonance regions, respectively, while the resulting piezoelectric signals were recorded using a lock-in amplifier with first harmonic (1*f*) demodulation. The measured frequency-response curves were normalized and fitted using Lorentzian functions, as shown in Fig. 5. The resonance frequencies of the fundamental and overtone modes were determined to be 2964.4 and 18294.0 Hz, respectively. The corresponding resonance linewidths were 0.86 and 3.53 Hz. According to $Q=f_{resonance}/\Delta f$, the Q-factors of the fundamental and overtone modes were calculated to be approximately 3447 and 5182, respectively. Compared with the simulated acoustic resonance frequencies of 2970 and 18300 Hz presented in Section 2.2, the measured QTF resonance frequencies exhibit mismatches of only 5.6 and 6.0 Hz, corresponding to relative deviations of approximately 0.189% and 0.0328%, respectively. These frequency mismatches are smaller than the corresponding half-power bandwidths of the acoustic resonances, indicating that both QTF vibration modes operate within the effective acoustic resonance ranges. However, the fundamental-mode frequency was located close to the lower 3 dB boundary of the acoustic resonance, making this channel more sensitive to frequency detuning than the overtone-mode channel. Nevertheless, the slight frequency deviations have a limited influence on the acoustic enhancement performance of the two sensing channels.

The two resonance frequencies are separated by more than 15 kHz, which provides sufficient frequency-domain separation for the two QEPAS sensing channels. Based on the 2*f* wavelength modulation scheme, the modulation frequencies for C_2H_2 and CH_4 detection were

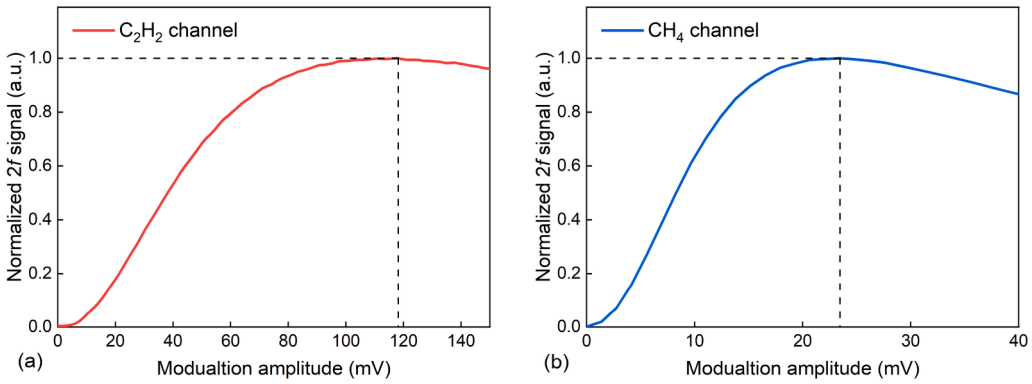


Fig. 6. Normalized 2 *f* signal amplitude as a function of the modulation amplitude for (a) C_2H_2 and (b) CH_4.

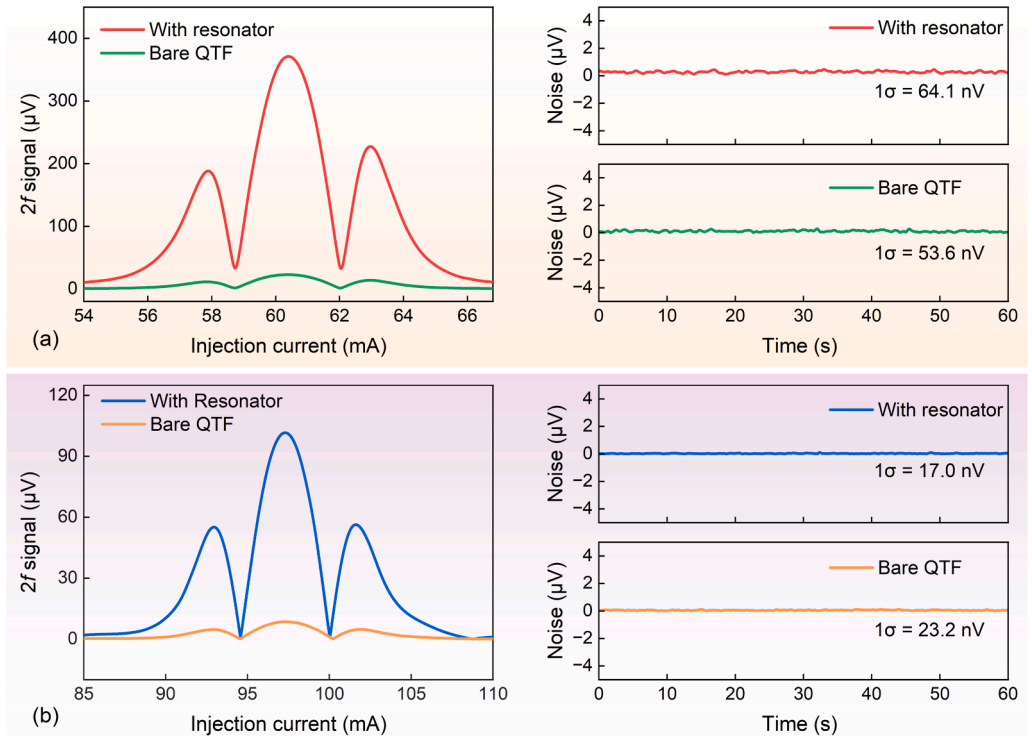


Fig. 7. Comparison of the QEPAS performance with and without the η-shaped acoustic resonator. (a) 2 *f* signals and corresponding noise levels for the C_2H_2 channel. (b) 2 *f* signals and corresponding noise levels for the CH_4 channel.

therefore set to half of the corresponding resonance frequencies, i.e., approximately 1482.2 and 9147.0 Hz, respectively.

After determining the operating frequencies, the modulation amplitudes of the two lasers were optimized to obtain the maximum 2 *f* signals. The optimization was performed independently at the respective operating frequencies of the two lasers, thereby accounting for differences in their effective wavelength-modulation responses under the experimental conditions. The sinusoidal modulation amplitude was gradually varied while the laser wavelength was fixed at the corresponding absorption lines. Fig. 6 shows the normalized 2 *f* signal amplitudes as functions of the modulation amplitude for the C_2H_2 and CH_4 channels. The signal amplitude initially increased with increasing modulation amplitude and subsequently decreased after reaching the optimum value. The maximum responses were obtained at modulation amplitudes of 118.2 mV for C_2H_2 and 23.5 mV for CH_4. These optimized parameters were used in the following experiments.

4.2. Dual-frequency acoustic enhancement

The acoustic enhancement performance of the η-shaped dual-resonance acoustic resonator was experimentally investigated by comparing its QEPAS responses with those obtained using a bare-QTF configuration. For the C_2H_2 and CH_4 channels, gas samples with concentrations of 20000 ppm and 18000 ppm were introduced into the gas cell, respectively. The 2 *f* signals were first recorded with the η-shaped acoustic resonator. For comparison, the same QTF was subsequently placed in a non-resonant gas cell. To ensure a reliable comparison, the laser powers, gas pressure, total flow rate, modulation parameters, and lock-in amplifier settings were kept unchanged for each sensing channel in both configurations. The total gas flow rate was maintained at 60 mL/min during the measurements. The background noise was evaluated by continuously recording the QTF output when the gas cell was filled with pure N_2. As shown in Fig. 7(a), the C_2H_2 2 *f* signal amplitude increased from 22.8 μV for the bare-QTF configuration to 371.2 μV with the η-shaped resonator, corresponding to a 16.3-fold signal enhancement.

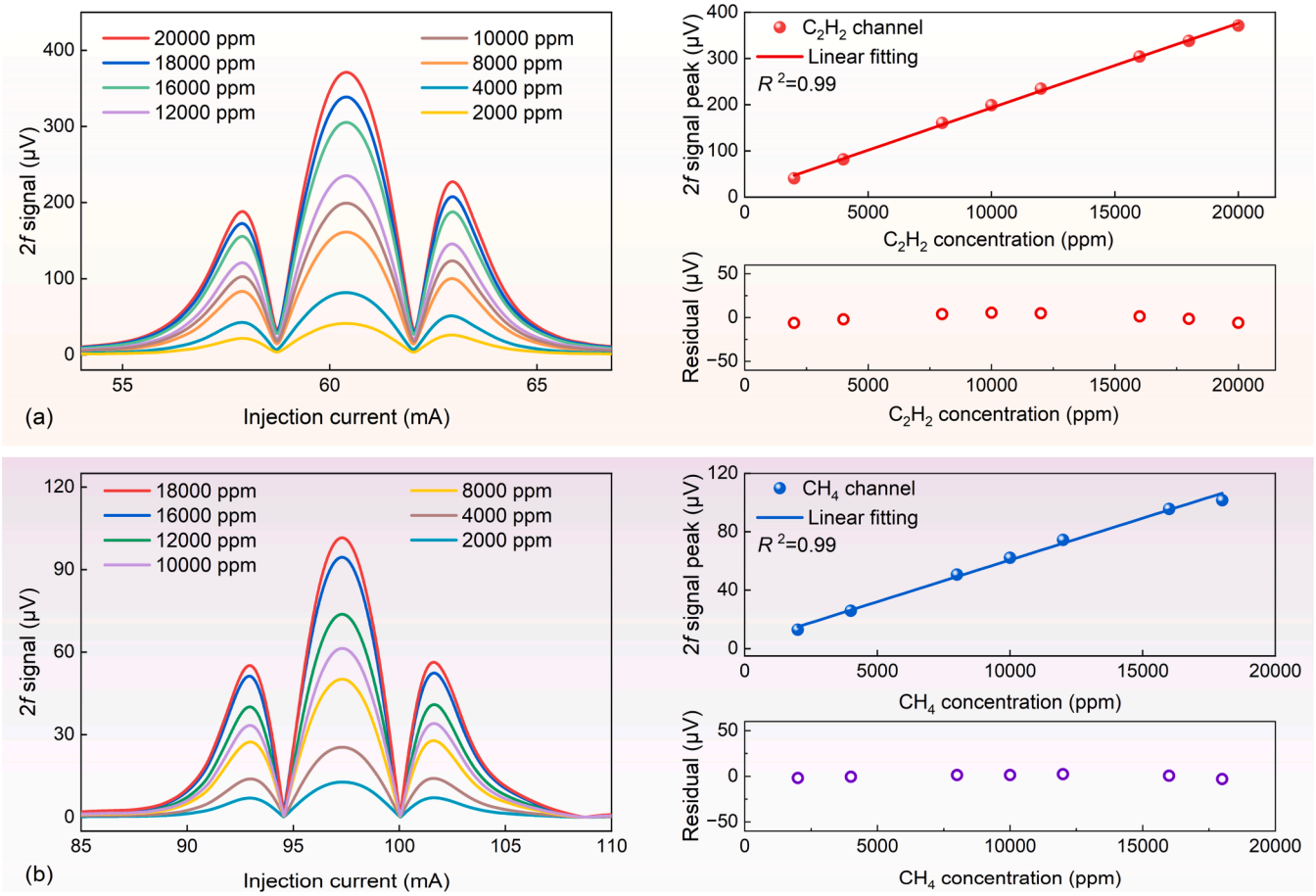


Fig. 8. Concentration responses of the dual-gas QEPAS sensor. (a) C_2H_2 2 *f* signals at different concentrations and the corresponding linear fitting. (b) CH_4 2 *f* signals at different concentrations and the corresponding linear fitting.

Meanwhile, the 1σ noise levels were 53.6 and 64.1 nV without and with the acoustic resonator, respectively. Thus, the corresponding signal-to-noise ratio (SNR) increased from approximately 425–5791, yielding an SNR enhancement factor of approximately 13.6. A similar enhancement was obtained for the CH_4 channel operating at the QTF overtone frequency. As shown in Fig. 7(b), the 2 *f* signal amplitude increased from 8.5 μV to 101.6 μV after introducing the η-shaped resonator, corresponding to a 12.0-fold enhancement. The measured 1σ noise levels for the bare-QTF and resonator-enhanced configurations were 23.2 and 17.0 nV, respectively. Accordingly, the SNR increased from approximately 366–5976, corresponding to an SNR improvement of approximately 16.3 times.

These results demonstrate that the η-shaped resonator provides considerable acoustic enhancement at both QTF resonance frequencies, with only modest changes in the background noise levels. Although a slight noise increase was observed in the C_2H_2 channel, the substantial signal enhancement resulted in significant SNR improvements for both gas species. More importantly, the enhancement is simultaneously available for the fundamental and overtone mode sensing channels, confirming the effectiveness of the dual-resonance design. Compared with the bare-QTF configuration, the enhanced acoustic pressure substantially improves the detection SNR for both gas species. Therefore, the proposed η-shaped structure provides an effective approach to achieve acoustic resonance enhancement in a frequency-multiplexed dual-gas QEPAS sensor using a single QTF.

4.3. Simultaneous dual-gas sensing and channel independence

To characterize the concentration response of the dual-gas sensor,

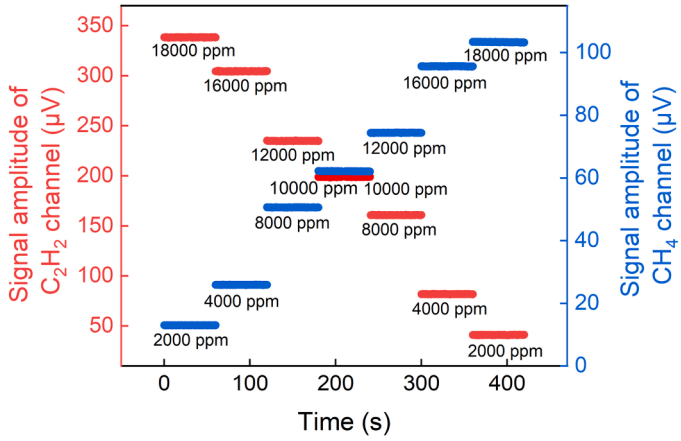


Fig. 9. Simultaneous concentration responses of C_2H_2 and CH_4 acquired by the η-shaped dual-resonance QEPAS sensor.

C_2H_2 and CH_4 samples with different concentrations were prepared by dynamic dilution using mass-flow controllers. The 2 *f* spectra were recorded at a series of gas concentrations, and the corresponding peak amplitudes were extracted for linear fitting. Fig. 8 shows the measured 2 *f* signals and concentration responses of the C_2H_2 and CH_4 channels. For both gas species, the 2 *f* signal amplitude increased monotonically with increasing gas concentration. The extracted 2 *f* peak amplitudes exhibited good linear dependences on the gas concentrations, with coefficients of determination R^2 higher than 0.99 for both sensing

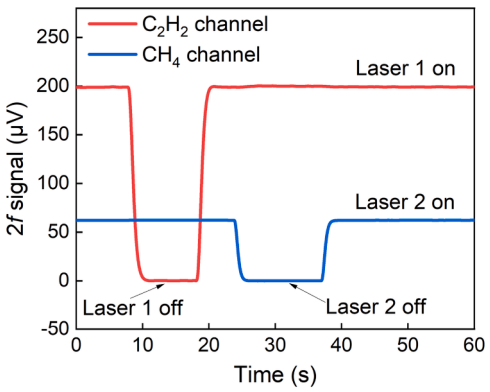


Fig. 10. Crosstalk characterization between the C_2H_2 and CH_4 sensing channels by alternately blocking the two excitation lasers.

channels. The fitting residuals of both channels were distributed around zero without an obvious concentration-dependent trend. These results further confirm the good linear concentration responses of the two sensing channels over the investigated ranges.

The capability of the sensor for simultaneous dual-gas measurement was further investigated by operating both excitation lasers at the same time. The wavelengths of the two lasers were fixed at the corresponding absorption lines, respectively. During the measurement, the CH_4 concentration was gradually increased from 2000 to 18000 ppm, while the C_2H_2 concentration was simultaneously decreased from 18000 to 2000 ppm. The two 2 *f* signals were continuously recorded during the concentration variation. As shown in Fig. 9, the CH_4 sensing channel signal increased stepwise with increasing concentration, whereas the C_2H_2 channel signal decreased correspondingly with decreasing concentration. The independent variation of the two signals demonstrates that the fundamental and overtone frequency channels can be simultaneously used for quantitative detection of different gas species.

Since two acoustic resonance channels coexist in the same η-shaped structure, the possible crosstalk between them was further evaluated. A gas mixture containing 10000 ppm C_2H_2 and 10000 ppm CH_4 was introduced into the resonator, while the two excitation lasers were independently blocked during continuous signal acquisition. When laser 1 (for C_2H_2 detection) was blocked, the C_2H_2 signal decreased to the laser-blocked background level, whereas the CH_4 signal remained essentially unchanged. Similarly, blocking laser 2 (for CH_4 detection) reduced the CH_4 signal to its corresponding background level without producing an observable variation in the C_2H_2 channel. Here, the laser-blocked background level refers to the residual lock-in signal measured when the corresponding excitation laser was blocked while the other laser remained in operation (Fig. 10).

The results indicate that no measurable inter-channel crosstalk was observed under the tested conditions. Although the two acoustic branches share a common buffer chamber and a certain degree of acoustic coupling may exist, the large frequency separation between the fundamental and overtone modes enables the corresponding signals to be independently extracted. Therefore, the experimental results confirm that the introduction of the dual-resonance acoustic structure does not compromise the channel independence required for simultaneous frequency-multiplexed QEPAS sensing under the investigated conditions.

4.4. *Long-term stability and detection limit*

Finally, the long-term stability of the dual-gas QEPAS sensor was evaluated using Allan deviation analysis. Pure N_2 was continuously introduced into the gas cell, while the background 2 *f* signals of the C_2H_2 and CH_4 channels were simultaneously recorded for more than 2 h. The acquired data were subsequently processed as a function of averaging time to evaluate the achievable detection limits. As shown in Fig. 11(a), the Allan deviation of the C_2H_2 channel continuously decreased with increasing averaging time and reached a minimum detection limit (MDL) of 148.7 ppb at an averaging time of 800 s. For the CH_4 channel, the Allan deviation decreased to an MDL of 155.0 ppb at an averaging time of 200 s, as shown in Fig. 11(b). At longer averaging times, the Allan deviations no longer continuously decreased, indicating the increasing contribution of long-term drift to the sensor noise. The Allan deviation results confirm the good long-term stability of both sensing channels and demonstrate that signal averaging can further improve the detection sensitivity. The achieved ppb level detection limits for both C_2H_2 and CH_4, together with the considerable acoustic enhancement and negligible inter-channel crosstalk, verify the feasibility of the η-shaped dual-resonance acoustic resonator for simultaneous and highly sensitive dual-gas QEPAS sensing using a single QTF.

5. Conclusion

In conclusion, we demonstrated a novel dual-gas QEPAS sensor based on an η-shaped dual-resonance acoustic resonator and a single low-frequency QTF. The fundamental and overtone modes of the QTF, with resonance frequencies of 2964.4 and 18294.0 Hz, were employed as two independent sensing channels. The η-shaped resonator provided simultaneous acoustic enhancement for both channels, increasing the C_2H_2 and CH_4 2 *f* signal amplitudes by 16.3 and 12.0 times, respectively. Both channels exhibited excellent linear responses with $R^2 > 0.99$, and no measurable inter-channel crosstalk was observed. Allan deviation analysis yielded MDLs of 148.7 ppb for C_2H_2 at 800 s and 155.0 ppb for CH_4 at 200 s. These results demonstrate that the proposed dual-resonance acoustic enhancement provides a simple and effective approach for improving the performance of single-QTF frequency-

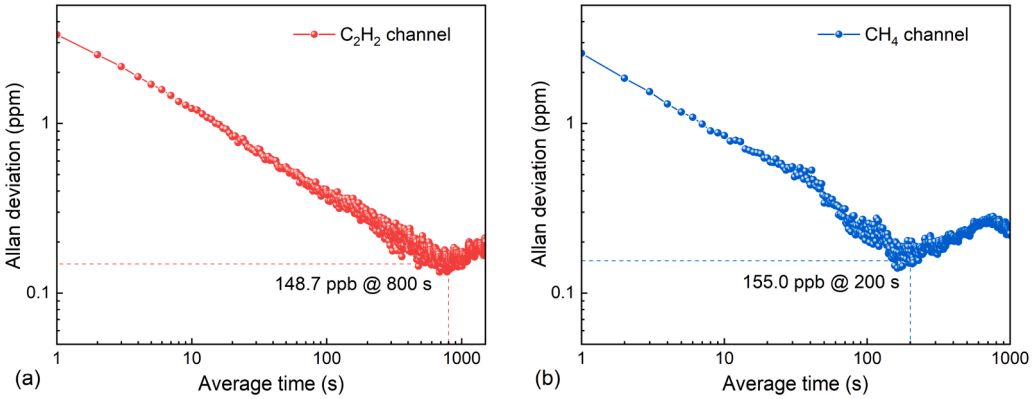


Fig. 11. Allan deviation analysis of the η-shaped dual-resonance QEPAS sensor for (a) C_2H_2 and (b) CH_4 detection.

multiplexed QEPAS sensors for multicomponent gas sensing.

CRediT authorship contribution statement

Zhen Zhang: Writing – original draft, Validation, Methodology, Investigation, Data curation. **Chenzhao Sang:** Visualization, Software, Investigation, Data curation. **Haiyue Sun:** Methodology, Formal analysis. **Chu Zhang:** Resources, Formal analysis. **Shunda Qiao:** Resources, Formal analysis. **Hong Qi:** Resources, Formal analysis. **Angelo Sampaolo:** Writing – review & editing, Formal analysis. **Vincenzo Spagnolo:** Writing – review & editing, Formal analysis. **Yufei Ma:** Writing – review & editing, Supervision, Resources, Project administration, Funding acquisition, Conceptualization. **Ying He:** Writing – review & editing, Visualization, Validation, Resources, Project administration, Methodology, Investigation, Funding acquisition, Formal analysis, Conceptualization.

Declaration of Competing Interest

The authors declare that they have no known competing financial interests or personal relationships that could have appeared to influence the work reported in this paper.

Acknowledgments

This research was funded by the National Natural Science Foundation of China (Grant No. 62335006, 62275065, 625B2063, 624B2050, 62022032, 62405078, and 62505066), Natural Science Foundation of Heilongjiang Province (Grant No. BS2025F002 and LH2024F031), Heilongjiang Postdoctoral Fund (Grant No. LBH-Z23144 and LBH-Z24155), China Postdoctoral Science Foundation (Grant No. 2024M764172), Open Subject of Hebei Key Laboratory of Advanced Laser Technology and Equipment (HBKL-ALTE2025001), and the Fundamental Research Funds for the Central Universities (HIT.DZJJ.2025015 and HIT.NSFJG202463).

Data availability

Data will be made available on request.

References

[1] S. Schilt, L. Thevenaz, M. Nikles, L. Emmenegger, C. Huglin, Ammonia monitoring at trace level using photoacoustic spectroscopy in industrial and environmental applications, Spectroc. Acta Pt. A-Molec. BioMolec. Spectr. 60 (2004) 3259–3268.
[2] C. Liu, M. Xu, M. Hu, S. Pan, H. Qi, S. Liu, H. Li, C. Liu, Y. Shang, CW DFB-QCL-based system for H_2O_2 detection using multi-pass tunable diode laser absorption spectroscopy, Chin. Opt. Lett. 23 (2025) 083001.
[3] J. Mu, Y. He, S. Qiao, H. Sun, Y. Ma, Antenna-inspired bionic lithium niobate tuning fork for multi-component light-induced thermoelastic spectroscopy sensing, Laser Photonics Rev. (2026) e71876, https://doi.org/10.1002/lpor.71876.
[4] M. Filonchyk, M. Peterson, L. Zhang, V. Hurynovich, Y. He, Greenhouse gases emissions and global climate change: examining the influence of CO_2, CH_4, and N_2O, Sci. Total. Environ. 935 (2024) 173359.
[5] B. Liu, G. Han, R. Wang, X. Yang, H. Sun, S. Qiao, Y. He, A. Sampaolo, V. Spagnolo, Y. Ma, Windmill-shaped multi-unit piezoelectric ceramic tuning fork for cooperatively enhanced photoacoustic methane sensing, Opto-Electron. Sci. 5 (2026) 260068.
[6] Y. Zhang, E. Yang, H.H. Yoon, Q. Cheng, Z. Sun, T. Hasan, W. Cai, Reconstructive spectrometers: hardware miniaturization and computational reconstruction, eLight 5 (2025) 23.
[7] H. Ma, S. Qiao, Y. He, H. Sun, Y. Ma, Orthogonal phase modulation and Lissajous mode decoupling in light-induced thermoelastic spectroscopy for real-time multi-component gas sensing, Rep. Prog. Phys. 89 (2026) 067902.
[8] T. Wildi, T. Voumard, V. Brasch, G. Yilmaz, T. Herr, Photo-acoustic dual-frequency comb spectroscopy, Nat. Commun. 11 (2020) 4164.
[9] X. Yin, Q. Hu, X. Yang, K. Xu, Y. Liang, J. Hou, A. Sampaolo, P. Patimisco, V. Spagnolo, D. Zhang, Z. Liu, H. Xu, H. Wu, Ppb-level HF sensor in GeF_4 gas matrices with a 76 m TDLAS cell, Sens. Actuators B Chem. 449 (2026) 139141.
[10] Y. Ma, X. Sun, H. Sun, Y. He, S. Qiao, An ultra-highly sensitive LITES sensor based on multi-pass cell with ultra-dense spot pattern designed by multi-objective algorithm, PhotoniX 6 (2025) 26.
[11] H. Sun, S. Qiao, Y. He, X. Sun, Y. Ma, Parts-per-quadrillion level gas molecule detection: CO-LITES sensing, Light. Sci. Appl. 14 (2025) 180.
[12] X. Ren, J. Pan, M. Yan, J. Sheng, C. Yang, Q. Zhang, H. Ma, Z. Wen, K. Huang, H. Wu, H. Zeng, Dual-comb optomechanical spectroscopy, Nat. Commun. 14 (2023) 5037.
[13] D. Wen, H. Zhao, X. Liu, M. Xu, X. Xu, X. Lei, R. Shu, Quantitative detection of water/ice in typical lunar minerals using Raman spectroscopy, J. Infrared Millim. Waves 44 (2025) 192–202.
[14] L. Fürst, M. Pal, A. Eber, E. Hruska, C. Hofmann, I. Gordon, M. Schultze, R. Breinbauer, B. Bernhardz, Free-running ultraviolet dual comb spectroscopy enabling absolute electronic fingerprinting, PhotoniX 7 (2026) 33.
[15] B. Liu, G. Han, Y. He, S. Qiao, R. Wang, H. Sun, Y. Ma, Owl-inspired dual-ended asymmetric lithium niobate tuning fork for high-sensitivity dual-gas laser spectroscopic sensing, Photonics Res. 14 (2026) 4579–4595.
[16] Y. Li, Y. Wang, Z. Liu, Y. Guo, X. He, Y. Zhao, Y. Liang, Z. Xu, J. Li, G. Zhao, M. Li, Y. Rao, T. Tan, B. Yao, Gas mapping based-on dual microcomb driven nanomaterial functionalized fiber Bragg grating string, PhotoniX 7 (2026) 4.
[17] H. Sun, S. Qiao, Y. He, Y. Wang, J. Hou, C. Zhang, Y. Dong, Y. Ma, High-speed and high-sensitivity multi-gas detection based on parallel heterodyne LITES sensor, Light. Sci. Appl. 15 (2026) 295.
[18] D. Nguyen, D. Kim, G. Lee, S. Kim, D. Shin, J. Park, H. Choi, S. Kim, S. Kim, Y. Kim, Real-time monitoring of fast gas dynamics with a single-molecule resolution by frequency-comb-referenced plasmonic phase spectroscopy, PhotoniX 5 (2024) 22.
[19] Y. Ma, Y. He, Y. Tong, X. Yu, F. Tittel, Quartz-tuning-fork enhanced photothermal spectroscopy for ultra-high sensitive trace gas detection, Opt. Express 26 (2018) 32103–32110.
[20] H. Ma, J. Cai, S. Qiao, Y. He, Y. Dong, Y. Ma, Dual-gas light-induced thermoelastic spectroscopy sensor based on mixed frequency heterodyne demodulation, Light. Adv. Manuf. 7 (2026) 54.
[21] Y. Song, S. Qiao, H. Ma, Y. He, Y. Ma, Gas sensing based on heterodyne Mach−Zehnder interferometric phase-dispersion spectroscopy, Anal. Chem. 98 (2026) 29627–29638.
[22] H. Chen, R. Zhao, X. Bi, N. Shen, X. Mo, Y. Tao, Z. Chen, J. Ye, Bacterial identification by metabolite-level interpretable surface-enhanced Raman spectroscopy, Adv. Photonics 7 (2025) 046007.
[23] Y. Huang, H. Sun, S. Qiao, Y. He, J. Hou, Y. Ma, Self-supervised deep learning for denoising in light-induced thermoelastic spectroscopy using 2D homologous 2*f* spectral matrices, Laser Photonics Rev. (2026) e71785, https://doi.org/10.1002/lpor.71785.
[24] S. Qiao, Z. Lang, Y. He, X. Zhi, Y. Ma, Calibration-free measurement of absolute gas concentration and temperature via light-induced thermoelastic spectroscopy, Adv. Photonics 7 (2025) 066007.
[25] Z. Zhao, V. Kravtsov, Z. Wang, Z. Zhou, L. Dou, D. Huang, Z. Wang, X. Cheng, M. Raschke, T. Jiang, Applications of ultrafast nano-spectroscopy and nano-imaging with tip-based microscopy, eLight 5 (2025) 1.
[26] Z. Zhuang, X. Zhou, H. Zeng, M. Li, Z. Chen, X. He, X. Chen, L. Zhou, J. Dong, Overcoming intrinsic dispersion locking for achieving spatio-spectral selectivity with misaligned bilayer metagratings, eLight 5 (2025) 13.
[27] X. Shen, Y. Zhang, R. Cui, D. Tian, M. Cheng, P. Patimisco, A. Sampaolo, C. Sun, X. Yin, V. Spagnolo, L. Dong, H. Wu, A sulfur dioxide detection platform based on photoacoustic spectroscopy and a 266.22 nm high-power stabilized LD-pumped solid-state Q-switched laser, Photoacoustics 42 (2025) 100702.
[28] L. Zhang, L. Liu, X. Zhang, X. Yin, H. Huan, H. Liu, X. Zhao, Y. Ma, X. Shao, T-type cell mediated photoacoustic spectroscopy for simultaneous detection of multi-component gases based on triple resonance modality, Photoacoustics 31 (2023) 100492.
[29] Z. Wang, Q. Nie, H. Sun, Q. Wang, S. Borri, P. Natale, W. Ren, Cavity-enhanced photoacoustic dual-comb spectroscopy, Light. Sci. Appl. 13 (2024) 11.
[30] G. Wu, Z. Gong, J. Ma, H. Li, M. Guo, K. Chen, W. Peng, Q. Yu, L. Mei, High-sensitivity miniature dual-resonance photoacoustic sensor based on silicon cantilever beam for trace gas sensing, Photoacoustics 27 (2022) 100386.
[31] X. Yang, Y. He, C. Zhang, S. Qiao, C. Wang, Y. Qu, Y. Ma, Skylark vocalization-inspired photoacoustic spectroscopy dual-component sensor based on a double-helix Helmholtz photoacoustic cell, Sens. Actuators B Chem. 467 (2026) 140602.
[32] B. Liu, S. Qiao, Y. He, Y. Ma, Single off-beam exciting dual-quartz-tuning-fork resonance-enhanced QEPAS trace gas sensing, Chin. Opt. Lett. 23 (2025) 103001.
[33] C. Sun, T. Yang, J. Zhang, H. Wang, B. Mo, H. Qi, K. Chen, Stepped-type photoacoustic resonator for simultaneous dual-gas detection, Anal. Chem. 98 (2026) 777–786.
[34] W. Wang, Z. Feng, Y. Jiang, J. Zhang, S. Yan, X. Cao, P. Lu, C. Sima, Topological optimization method "MMA-BP" for photoacoustic resonator and implementations in ppt-level gas sensor using miniaturized vase-type photoacoustic cells, Photoacoustics 46 (2025) 100767.
[35] X. Yang, C. Zhang, S. Qiao, Y. He, Y. Qu, Y. Ma, Non-resonant quartz-enhanced photoacoustic spectroscopy, Chin. Opt. Lett. 23 (2025) 093002.
[36] W. Wang, T. Zhang, Q. Zhang, Y. Feng, Y. Wei, L. Wang, Y. Gu, C. Li, Photoacoustic spectroscopy two-component gas sensing system based on a semi- ellipsoidal resonant photoacoustic cell, Sens. Actuators B Chem. 446 (2025) 138616.
[37] G. Wu, L. Zhang, Y. Guan, Z. Gong, T. Gao, J. Xing, M. Zhang, W. Peng, L. Mei, Dual-enhanced fiber-optic photoacoustic spectroscopy via asymmetric cavity coupling and cantilever amplification for sub-ppb C_2H_2 detection, Sens. Actuators B Chem. 458 (2026) 139827.
[38] G. Wu, Y. Guan, L. Zhang, T. Gao, Z. Gong, J. Xing, M. Zhang, W. Gao, Ultrasensitive single-fiber Fabry–Pérot photoacoustic acetylene sensor enabled by a T-type acoustic resonator, Anal. Chem. 98 (2026) 27235–27243.

[39] J. Wang, H. Wu, A. Sampaolo, P. Patimisco, V. Spagnolo, S. Jia, L. Dong, Quartz-enhanced multiheterodyne resonant photoacoustic spectroscopy, Light. Sci. Appl. 13 (2024) 77.
[40] S. Qiao, Z. Zhang, B. Liu, Z. Lv, Y. He, H. Sun, X. Zhi, Y. Dong, A. Sampaolo, V. Spagnolo, Y. Ma, Ultrasensitive laser spectroscopy gas sensing based on a quartz tuning fork with novel topological configuration, Opto-Electron. Adv. 9 (2026) 260192.
[41] Y. Song, S. Qiao, H. Ma, Y. He, Y. Ma, Quartz-tuning-fork-filtered heterodyne interferometric phase-dispersion gas sensing based on dual-channel Hilbert phase extraction, Laser Photonics Rev. (2026) e72042, https://doi.org/10.1002/lpor.72042.
[42] R. Zhao, X. Yang, B. Liu, C. Zhang, S. Qiao, Y. He, H. Sun, R. Yan, Y. Ma, Highly sensitive photoacoustic detection of methane based on a rhombic dual-channel differential photoacoustic cell, Laser Part. Beams 44 (2026) 20009.
[43] C. Twomey, G. Biagi, A. Ruth, F. Ali, A. Falco, L. O'Faolain, A. Walsh, Side-polished fiber evanescent wave quartz-enhanced photoacoustic spectroscopy employing dielectric coatings for evanescent field enhancement, Photoacoustics 46 (2025) 100782.
[44] R. Wang, Y. He, S. Qiao, B. Liu, C. Zhang, H. Sun, Y. Ma, An asymmetric quartz tuning fork for enhanced localized photothermal excitation in light-induced thermoelastic spectroscopy sensing, Sens. Actuators B Chem. 471 (2027) 141067.
[45] A. Sampaolo, P. Patimisco, M. Giglio, A. Zifarelli, H. Wu, L. Dong, V. Spagnolo, Quartz-enhanced photoacoustic spectroscopy for multi-gas detection: A review, Anal. Chim. Acta 1202 (2022) 338894.
[46] S. Qiao, X. Liu, Z. Lang, Y. He, W. Chen, Y. Ma, Quartz-enhanced laser spectroscopy sensing, Light. Sci. Appl. 15 (2026) 5.
[47] L. Melchiorre, F. Anelli, G. Menduni, A. Annunziato, L. Bodin, S. Cozic, G. Magno, A. Sampaolo, F. Prudenzano, V. Spagnolo, Dual-gas quartz-enhanced photoacoustic spectroscopy sensor exploiting two fiber-combined interband cascade lasers, Photoacoustics 42 (2025) 100689.
[48] S. Qiao, Y. He, H. Sun, P. Patimisco, A. Sampaolo, V. Spagnolo, Y. Ma, Ultra-highly sensitive dual gases detection based on photoacoustic spectroscopy by exploiting a long-wave, high-power, wide-tunable, single-longitudinal-mode solid-state laser, Light. Sci. Appl. 13 (2024) 100.
[49] H. Wu, L. Dong, X. Liu, H. Zheng, X. Yin, W. Ma, L. Zhang, W. Yin, S. Jia, Fiber-amplifier-enhanced QEPAS sensor for simultaneous trace gas detection of NH_3 and H_2S, Sensors 15 (2015) 26743–26755.
[50] L. Qin, S. Bi, R. Chen, Y. Zhao, J. Shi, H. Zhang, Z. Wang, Two-component gas sensor of time-division multiplexing technique based on QEPAS and LITES, IEEE Photonics Technol. Lett. 36 (2024) 1085–1088.
[51] Y. Fu, H. Zhang, S. Bi, J. Zhao, J. Shi, Y. Zhao, A quartz-enhanced photothermal spectroscopy for C_2H_2 and CH_4 detection based on time division multiplexing technology, IEEE Sens. J. 24 (2024) 34440–34447.
[52] Q. Zhang, J. Chang, Z. Cong, J. Sun, Z. Wang, QEPAS sensor for simultaneous measurements of H_2O, CH_4, and C_2H_2 using different QTFs, IEEE Photonics J. 10 (2018) 6804308.
[53] C. Wang, Z. Wang, X. Pang, Quartz-enhanced photoacoustic spectroscopy for four-component gas detection based on two off-beam acoustic microresonators, Front. Phys. 8 (2020) 594326.
[54] S. Qiao, Z. Lv, B. Liu, H. Ma, Y. He, H. Sun, Y. Ma, Asymmetric tongs induced frequency splitting achieving simultaneous two-component gas sensing with a single quartz tuning fork in two independent resonant modes, ACS Sens. 11 (2026) 7104–7114.
[55] Z. Zhang, X. Zhang, X. Liu, L. Qin, S. Bi, Z. Wang, Detection of CH_4 and C_2H_2 utilizing frequency division multiplexing based on two-on-beam quartz- enhanced photoacoustic spectroscopy technology, Infrared Phys. Technol. 152 (2026) 106260.
[56] H. Wu, X. Yin, L. Dong, K. Pei, A. Sampaolo, P. Patimisco, H. Zheng, W. Ma, L. Zhang, W. Yin, L. Xiao, V. Spagnolo, S. Jia, F. Tittel, Simultaneous dual-gas QEPAS detection based on a fundamental and overtone combined vibration of quartz tuning fork, Appl. Phys. Lett. 110 (2017) 121104.
[57] M. Olivieri, A. Elefante, G. Menduni, M. Giglio, H. Wu, L. Dong, P. Patimisco, V. Spagnolo, A. Sampaolo, Simultaneous detection of $^{12}CH_4$, $^{13}CH_4$, and related isotope ratio exploiting a frequency-multiplexed mid-infrared quartz-enhanced photoacoustic sensor, ACS Sens. 11 (2026) 247–256.
[58] R. Rousseau, Z. Loghmari, M. Bahriz, K. Chamassi, R. Teisser, A. Baranov, A. Vicet, Off-beam QEPAS sensor using an 11-μm DFB-QCL with an optimized acoustic resonator, Opt. Express 27 (2019) 7435–7446.
[59] I.E. Gordon, L.S. Rothman, R.J. Hargreaves, R. Hashemi, E.V. Karlovets, F. M. Skinner, E.K. Conway, C. Hill, R.V. Kochanov, Y. Tan, P. Wcisło, A.A. Finenko, K. Nelson, P.F. Bernath, M. Birk, V. Boudon, A. Campargue, K.V. Chance, A. Coustenis, B.J. Drouin, J.–M. Flaud, R.R. Gamache, J.T. Hodges, D. Jacquemart, E.J. Mlawer, A.V. Nikitin, V.I. Perevalov, M. Rotger, J. Tennyson, G.C. Toon, H. Tran, V.G. Tyuterev, E.M. Adkins, A. Baker, A. Barbe, E. Canè, A.G. Császár, A. Dudaryonok, O. Egorov, A.J. Fleisher, H. Fleurbaey, A. Foltynowicz, T. Furtenbacher, J.J. Harrison, J.–M. Hartmann, V.–M. Horneman, X. Huang, T. Karman, J. Karns, S. Kassi, I. Kleiner, V. Kofman, F. Kwabia–Tchana, N. N. Lavrentieva, T.J. Lee, D.A. Long, A.A. Lukashevskaya, O.M. Lyulin, V. Y. Makhnev, W. Matt, S.T. Massie, M. Melosso, S.N. Mikhailenko, D. Mondelain, H. S.P. Müller, O.V. Naumenko, A. Perrin, O.L. Polyansky, E. Raddaoui, P.L. Raston, Z. D. Reed, M. Rey, C. Richard, R. Tóbiás, I. Sadiek, D.W. Schwenke, E. Starikova, K. Sung, F. Tamassia, S.A. Tashkun, J. Vander Auwera, I.A. Vasilenko, A.A. Vigasin, G.L. Villanueva, B. Vispoel, G. Wagner, A. Yachmenev, S.N. Yurchenko, The HITRAN2020 molecular spectroscopic database, J. Quant. Spectrosc. Radiat. Transf. 277 (2022) 107949.
[60] H. Qi, X. Zhao, W. Liu, C. Li, X. Zhang, M. Guo, K. Chen, Simultaneous detection of dual-component gases using a single multipass photoacoustic cell with cross-patterned spots, Anal. Chem. 98 (2026) 13049–13055.
[61] C. Sun, J. Zhang, H. Wang, C. Li, X. Han, H. Qi, K. Chen, Fiber-optic photoacoustic dual-gas analyzer based on a symmetric four-cone converging cell with dual-frequency resonance, Anal. Chem. 98 (2026) 29312–29321.

Zhen Zhang received his B.S. degree in Electronic Science and Technology from Harbin Institute of Technology in 2006, and M.S. degree in Physical Electronics from Harbin Institute of Technology in 2008. He is currently pursuing a PhD degree in Electronic Information at Harbin Institute of Technology.

Chenzhao Sang obtained his B.S. degree in Optoelectronic Information Science and Engineering from Dalian Minzu University, China, in 2024. He is now pursuing a M.S. degree in Electronic Information from Harbin Institute of Technology. His research interest is photoacoustic spectroscopy sensing.

Haiyue Sun obtained his B.S. degree in electronic science and technology from Harbin Institute of Technology, China, in 2018. In 2020, he received his M.S. degree in physical electronics from Harbin Institute of Technology. He is now pursuing a PhD degree of physical electronics from Harbin Institute of Technology. His research interest is light-induced thermoelastic spectroscopy.

Chu Zhang received her B.S. degree in Qingdao University of Technology, China, in 2019. Then, she obtained a master's degree in control engineering from Northeastern University. She is now pursuing a Ph.D. degree of physical electronics from Harbin Institute of Technology. Her research interest is photoacoustic cell design based photoacoustic spectroscopy.

Shunda Qiao received his B.S. degree in electronic science and technology from Yanshan university, China, in 2018. In 2020, he received his M.S. degree and began to pursue a PhD degree of physical electronics from Harbin Institute of Technology. Currently, he is an associate professor at the Harbin Institute of Technology, China. His research interests include photoacoustic spectroscopy and its applications.

Hong Qi received his PhD degree in engineering thermophysics from Harbin Institute of Technology, China, in 2008. From October 2011 to October 2012, he spent a year as a visiting scholar at UCLA, USA. Currently, he is a professor at Harbin Institute of Technology, China. His research interests include photothermal radiation transfer and coupled heat transfer, measurement of photothermal radiation characteristics, and radiation inverse problem. He has published more than 100 papers and granted 45 patents. He serves as a member of the scientific council of ICHMT.

Angelo Sampaolo obtained his Master degree in Physics in 2013 and the PhD Degree in Physics in 2017 from University of Bari. He was an associate researcher in the Laser Science Group at Rice University from 2014 to 2016 and associate researcher at Shanxi University since 2018. Since 2024, he is Associate Professor at Polytechnic of Bari. His research activity has focused on the development of innovative techniques in trace gas sensing, based on Quartz-Enhanced Photoacoustic Spectroscopy.

Vincenzo Spagnolo received the degree (summa cum laude) and the PhD, both in physics, from University of Bari. He works as Full Professor of Applied Physics at the Technical University of Bari. In 2019, he become Vice-Rector of the Technical University of Bari, deputy to Technology Transfer. Since 2017, he is the director of the joint-research lab PolySense, created by THORLABS GmbH and Technical University of Bari, devoted to the development and implementation of novel gas sensing techniques and the realization of highly sensitive QEPAS trace-gas sensors.

Yufei Ma received his PhD degree in physical electronics from Harbin Institute of Technology, China, in 2013. From September 2010 to September 2011, he spent as a visiting scholar at Rice University, USA. Currently, he is a professor at Harbin Institute of Technology, China. He is an Optica Fellow and the winner of National Outstanding Youth Science Fund. His research interests include optical sensors, trace gas detection, laser spectroscopy, solid-state laser and optoelectronics. He has published more than 200 publications and given more than 50 invited presentations at international conferences. He serves as area editor for Elsevier *Photoacoustics* and Wiley *Microwave and Optical Technology Letters,* associate editor for *Optics Express*, SPIE *Optical Engineering*. He also serves as topical editor for *Optics Letters* and *Chinese Optics Letters*.

Ying He obtained his master and doctorate degrees in physical electronics from Harbin Institute of Technology in 2017 and 2022, respectively. Currently, he is an associate professor at the Harbin Institute of Technology, China. His research interests including trace gas sensing based on QEPAS, LITES and other laser spectroscopy.